ulm university universität
uulm

Fakultät für Naturwissenschaften

Institute of Theoretical Physics

The Effects of Casimir Interactions in Experiments on Gravitationally-induced Entanglement

Bachelor Thesis

Submitted by:
Jan Bulling
jan.bulling@uni-ulm.de
1109395

Supervised by:
Marit O. E. Steiner, Julen S. Pedernales, Martin B. Plenio

Abstract

Contents

1 Introduction

1.1 Feynman's Gedankenexperiment

2 A first look

Testing the quantum nature of gravity is no easy task and many proposals seek to detect gravitationally induced entanglement between two masses [1–4] as a form of proof. For all these proposals, gravity is assumed to be mediated by a gravitational field. During a time evolution, this field (like any other external field) can only perform local operations (LO) on the states of the test masses. If gravity is now assumed to behave classically, the propagation between the masses can be described by a classical communication (CC) channel [4, 5]. These LOCC operations however cannot turn an initially unentangled state into an entangled one [6, 7]. It immediately follows, that if one measures the involved masses to be entangled after a mutual gravitational interaction, gravity necessarily has to be quantum in some way. It is important to note, that the opposite of this statement is not true. Measuring unentangled masses does not directly imply the classicality of the gravitational field. This can be seen by considering operations that are non-LOCC and also produce unentangled states like for example the swap operation $|\psi\rangle_A |\phi\rangle_B \to |\phi\rangle_A |\psi\rangle_B$. This operations obviously can't induce entanglement to initially unentangled states, but requires the perfect exchange of quantum information between the states - which is not possible using classical communication alone. In other words: If one prepares masses initially in a pure product state and measures *any* state which cannot be obtained by LOCC-operations after some final time evolution, it is impossible for gravity to behave classical. One can even go so far and define the term ***quantum gravity*** as any interaction mediated by gravity that cannot be described by LOCC operations alone [5].

A plausible and logical idea for an experiment to test for gravitational induced entanglement is described in this chapter - which is, as a reminder, enough to prove a quantum nature of gravity. It requires the generation of coherent delocalized quantum superpositions of massive objects either as so-called Schrödinger-cat states or squeezed gaussian states [4, 8]. Theses masses are brought close enough together for gravity to have a measurable effect. The distances between different parts of the spatial superpositions must have different distances to the delocalized second mass. As a result - and of course *if gravity behaves quantum* - the states should get entangled. To see this, consider the ideal simplification of a real experimental setup where two bodies with mass m are trapped in an harmonic potential wall (like for example in an optical trap) with frequency ω separated by a distance d. The local Hamiltonian of the system is given by

$$\hat{H}_0 = \sum_{i=1,2} \frac{\hat{p}_i^2}{2m} + \frac{1}{2} m\omega^2 \hat{x}_i^2 \tag{2.1}$$

where $\hat{x}$ and $\hat{p}$ are the position and momentum operators satisfying the canonical com-

mutation relation $[\hat{x}_i, \hat{p}_j] = i\hbar\delta_{ij}$. For now, all non-gravitational interactions between the masses have been ignored. In the low energy regime, where the energy transfer during a process is far below the Planck scale $m_p c^2 \sim 10^{19}\,\mathrm{GeV}$, gravity can be traded as an effective field theory with tools available similar to those for the electromagnetic field and QED [9]. In the non-relativistic limit $v \ll c$, the gravitational interaction can be described by a Newtonian $1/r$ potential acting on the center-of-mass positions, with all classical quantities are replaced by quantum operators [8–10]. Spatial superpositions lead to superpositions of the metric and consequently (in the non-relativistic limit) to a superposed Newtonian potential. The interaction Hamiltonian $\hat{H}_G$ should therefore be describable by

$$\hat{H}_G = -\frac{Gm^2}{|d - \hat{x}_1 + \hat{x}_2|}, \tag{2.2}$$

where $G = 6.6743 \times 10^{-11}\,\mathrm{m^3 kg^{-1} s^{-2}}$ is the gravitational constant. The separation of the masses d is chosen much larger than the extension of the delocalization (in this setup comparable to the position variance of the harmonic oscillator). This condition is realistic given that the biggest spatial delocalization is in the order of !!!SOURCES!!!. Expanding the Hamiltonian $\hat{H}_G$ for small $\hat{x}_i$, only the second order term proportional to $(\hat{x}_1 - \hat{x}_2)^2$ can induce entanglement [1]. The zeroth order term is just a overall energy offset, the first order term $\propto (\hat{x}_1 - \hat{x}_2)$ as well as the terms $\hat{x}_i^2$ result only in a local interaction for each mass separately. The coupling term $-(\hat{x}_1\hat{x}_2 + \hat{x}_2\hat{x}_1) = -2\hat{x}_1\hat{x}_2$ however is very interesting as it couples both oscillators and can thus mediate entanglement. Introducing the ladder operators, the Hamiltonian $\hat{H} = \hat{H}_0 + \hat{H}_G$ can be expressed as [9]:

$$\hat{H} = \sum_{i=1,2} \hbar\omega \hat{a}_i^\dagger \hat{a}_i - \frac{Gm^2}{d^3}\left(\sqrt{\frac{\hbar}{2m\omega}}\right)^2 \left(\hat{a}_1\hat{a}_2 + \hat{a}_1\hat{a}_2^\dagger + \hat{a}_1^\dagger\hat{a}_2 + \hat{a}_1^\dagger\hat{a}_2^\dagger\right) \tag{2.3}$$

Applying the *rotating-wave approximation*[1], the terms $\hat{a}_1\hat{a}_2 + \hat{a}_1^\dagger\hat{a}_2^\dagger$ can be dropped. Defining the coupling strength g of the interaction as $g = Gm/\omega d^3$, eq (2.3) can be rewritten as

$$\hat{H} = \sum_{i=1,2} \hbar\omega \hat{a}_i^\dagger \hat{a}_i - \hbar g\left(\hat{a}_1\hat{a}_2^\dagger + \hat{a}_1^\dagger\hat{a}_2\right). \tag{2.4}$$

Now, for simplicity and as a simple example, the evolution of the initial Fock state $|\psi(0)\rangle = |10\rangle$ is considered. The gravitational interaction H_G can be treated as a time dependent perturbation and the state evolution is given as (for calculation see appendix A.1.1) [9]

$$|\psi(t=0)\rangle = |10\rangle \xrightarrow{\text{time } t} |\psi(t)\rangle = \mathcal{N}\left(|10\rangle - igt\,|01\rangle + \mathcal{O}(g^2)\right) \tag{2.5}$$

where $\mathcal{N}$ is an appropriate normalization constant. The evolved state (2.5) is entangled and cannot be reduced into a product of two oscillator Fock states. The entanglement

[1] This approximation is known from quantum optics, where all fast oscillating terms in the Hamiltonian can be dropped [5, 9]. In the interaction picture, the ladder operators evolve as $\hat{a}(t) = \hat{a}e^{-i\omega t}$. The terms like $\hat{a}_1(t)\hat{a}_2(t)$ oscillate with frequency 2ω whereas $\hat{a}_1^\dagger(t)\hat{a}_2(t)$ does not oscillate at all. Due to the small coupling, this approximation works very well here.

is very small since it is proportional to the gravitational coupling constant gt [2] but can still be measured by ???? !!!SOURCES!!!. Another interesting result, which underlines the false inference of a classical gravity from observed non-entanglement discussed above can be seen by considering the time evolution of a coherent product state $|\alpha\rangle \otimes |\beta\rangle$ where $\hat{a}\,|\alpha\rangle = \alpha\,|\alpha\rangle$. The time evolution is derived in appendix A.1.2 and results in

$$e^{-i\hat{H}t/\hbar}\left(|\alpha\rangle \otimes |\beta\rangle\right) = \left|e^{-i\omega t}\left(\alpha\cos gt - \beta\sin gt\right)\right\rangle \otimes \left|e^{-i\omega t}\left(-\alpha\sin gt + \beta\cos gt\right)\right\rangle . \quad (2.6)$$

This state is clearly a product state and thus not entangled. But for a time $t_0 = \pi/2g$ the state is effectively the swapped initial state $|\beta\rangle \otimes |\alpha\rangle$ up to a local phase. This swap operation is however, as established earlier, not possible under a LOCC protocol. Thus, even if the resulting state after time evolution under a gravitational interaction is unentangled, we can role out the classicality of gravity [5, 9]. Gravity must therefore be capable of transmitting quantum information and must be described by a quantum channel.

Experimentally, one requires the ability to generate spatial superpositions of two massive objects with large enough coherence times. Usually the weak gravitational interaction requires coherence times in the order of $100\,\mathrm{ms} - 10\,\mathrm{s}$ for any meaningful and measurable entanglement to built up. The masses should additionally be massive enough for their gravitational effects to be measurable. These requirements impose huge experimental and engineering challenges. To contextualize: The most massive object ever put into a spatial superposition is in the order of $4 \times 10^{-23}\,\mathrm{kg}$, whereas the smallest object whose gravitational field has been measured was just below 100 mg [11] - a difference of 19 orders of magnitude. One way to experimentally create such spatial superpositions is giving the masses a spin-1/2 degree of freedom. For example, a nitrogen-vacancy diamonds can be used [4], where the NV site provides the required spin of 1/2. An applied magnetic gradient $\partial_x B$ functions like a "beam splitter" and creates a delocalized state. The extend of this superposition can be calculated and separations in the order of $100\,\mu\mathrm{m}$ are theoretically achievable [4]. Levitated, trapped particles isolated and shielded in a vacuum can increase environmental isolation by avoiding contact with surrounding noise. The additional forces due to the trapping potential or the gravitational acceleration can be studied in advance. In this thesis, I assume that all required states and superpositions can be prepared experimentally.

The general and idealized problem considered is illustrated in fig. 2.1. Two massive bodies with masses M_A and M_B are initially separated by a center-to-center distance $2L$. The masses are prepared in a coherent delocalized quantum superposition Schrödinger-cat-like state in, for now, a parallel orientation as depicted in fig. 2.1. The extension of the superposition is denoted by Δx and is the same for both masses. It is important to choose the positions of the masses such that the distances between each part of the delocalized mass A and B are not always identical. Otherwise, all built up phases are the same and no entanglement is observable. With the notation introduced in fig. 2.1,

[2] The amount of entanglement can for example be measured with the later introduced *logarithmic negativity* E_N. For this state, this quantity is given as $E_N(|\psi(t)\rangle\langle\psi(t)|) \simeq 2tg/\log 2 + \mathcal{O}(g^2) \geq 0$.

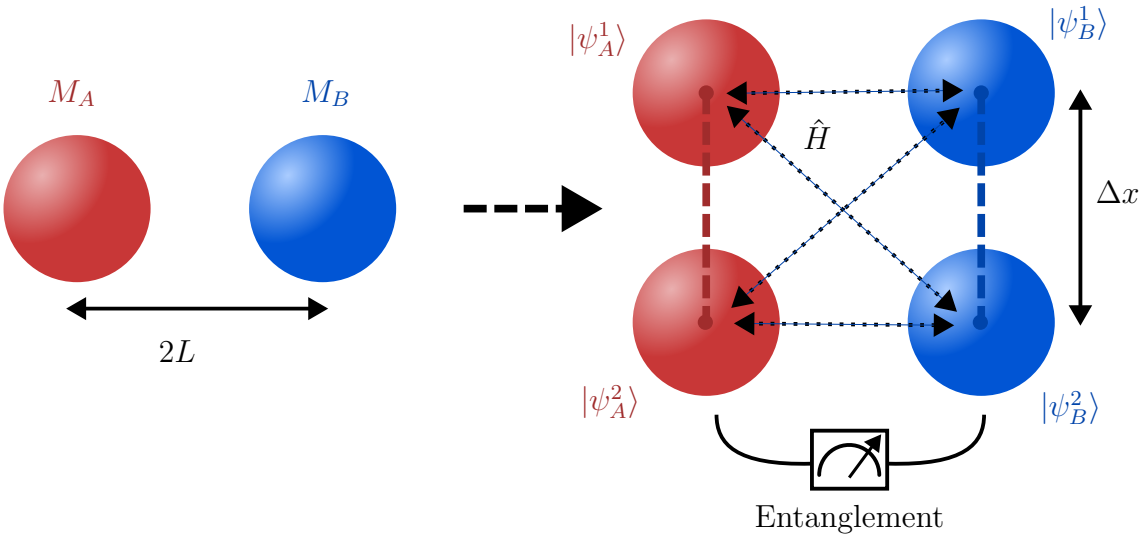

Figure 2.1: Schematic figure of the proposed experiment with two masses prepared in a spatial superposition state. The gravitational interaction $\hat{H}$ induces different phases to each of the superpositions due to the different distances between all masses. This results in measurable entanglement after some time evolution.

the initial state at $t = 0$ is given by

$$|\psi(t=0)\rangle = \frac{1}{2}\left(\left|\psi_A^1\right\rangle + \left|\psi_A^2\right\rangle\right) \otimes \left(\left|\psi_B^1\right\rangle + \left|\psi_B^2\right\rangle\right). \tag{2.7}$$

The state evolves under a Hamiltonian $\hat{H}$ and after some time the position of each mass is measured and checked for entanglement. For now I assume that all interactions except gravity can be neglected. In reality, electromagnetic forces and Casimir-Polder interactions [12, 13] need to be considered.

As established earlier in this chapter, with some assumptions made, gravitational interaction can generate entanglement. In the time scales of the experiment, the acceleration of the masses due to the mutual gravitational interaction can be neglected [3]. The Hamiltonian therefore only needs to include the gravitational potential

$$\hat{V} = -\frac{GM_AM_B}{\left|\hat{D}\right|} \tag{2.8}$$

where $\hat{D}$ is the distance operator between the masses. It depends on the individual positions $\hat{x}_A$ and $\hat{x}_B$. During time evolution, the different parts of the superpositions built up different local phases. I am interested in calculating, how much entanglement one can expect from this kind of interactions.

[3] Take for example a silica sphere ($\rho = 2648\,\mathrm{kg/m^3}$) with $R = 10^{-5}\,\mathrm{m}$ separated by $L = 2R$. The mutual gravitational acceleration for each sphere is around $a = GM/(2L)^2 = 5 \times 10^{-13}\,\mathrm{m/s^2}$ which results for $t \sim 1\,\mathrm{s}$ in a distance traveled of $\sim 10^{-13}\,\mathrm{m}$.

2.1 Time evolution under a gravitational potential

Proposition 2.1. *The time evolution under a static and constant Hamiltonian* $\hat{H} = \hat{V}(\hat{x}_i) = \text{const.}$ *is given by the eigenenergies of the system* $\hat{V}\left|n\right\rangle = V_n\left|n\right\rangle$ *proportional to* $e^{-iV_nt/\hbar}$.

Proof. This is a trivial statement. The time evolution is governed by the Schrödinger equation

$$i\hbar\frac{\partial}{\partial t}\left|\psi(t)\right\rangle = \hat{H}\left|\psi(t)\right\rangle. \tag{2.9}$$

The formal solution of this first order PDE is given by

$$\left|\psi(t)\right\rangle = e^{-i\hat{V}t/\hbar}\left|\psi(t=0)\right\rangle. \tag{2.10}$$

The constant (hermitian) potential operator can be expressed in the energy-eigenbasis $\{\left|n\right\rangle\}$ as $\hat{V}\left|n\right\rangle = V_n\left|n\right\rangle$. The initial state can be expressed as a superposition in the same eigenstates like $\left|\psi\right\rangle = \sum_n c_n\left|\psi_n\right\rangle$. Putting both together and using the taylor expansion of the exponential function, one arrives at the simple form

$$\left|\psi(t)\right\rangle = \sum_n e^{-i\hat{V}t/\hbar}\left|n\right\rangle\left\langle n|\psi\right\rangle = \sum_{n,k}\frac{(-i\hat{V}t/\hbar)^k}{k!}\left|n\right\rangle c_n\left|\psi_n\right\rangle \tag{2.11}$$

$$= \sum_{n,k}\frac{(-iV_nt/\hbar)^k}{k!}c_n\left|\psi_n\right\rangle = \sum_n e^{-iV_nt/\hbar}c_n\left|\psi_n\right\rangle \tag{2.12}$$

where in the second to last step $\hat{V}^k\left|n\right\rangle = \hat{V}^{k-1}\hat{V}\left|n\right\rangle = \hat{V}^{k-1}\left|n\right\rangle V_n = \cdots = V_n^k\left|n\right\rangle$ was used. □

Using the preceding proposition, the initial state eq. (2.7) can be evolved in time. The potential operator eq. (2.8) acts on every state in the $\{\left|\psi_A^1\right\rangle, \left|\psi_A^2\right\rangle\} \otimes \{\left|\psi_B^1\right\rangle, \left|\psi_B^2\right\rangle\}$ basis differently. This is because of the different distances between the states $\left|\psi_A^i\right\rangle$ and $\left|\psi_B^j\right\rangle$ for different $i, j \in \{1, 2\}$. This results in phases ϕ_{ij} to be built up during time evolution according to proposition 2.1. The state $\left|\psi(t)\right\rangle$ after some time evolution is therefore given as

$$\left|\psi(t)\right\rangle = \frac{1}{2}\Big(e^{i\phi_{11}}\left|\psi_A^1\right\rangle\left|\psi_B^1\right\rangle + e^{i\phi_{12}}\left|\psi_A^1\right\rangle\left|\psi_B^2\right\rangle + e^{i\phi_{21}}\left|\psi_A^2\right\rangle\left|\psi_B^1\right\rangle + e^{i\phi_{22}}\left|\psi_A^2\right\rangle\left|\psi_B^2\right\rangle\Big), \tag{2.13}$$

where the $\otimes$ symbol was omitted. The phases are

$$\phi \equiv \phi_{11} = \phi_{22} = \frac{GM_AM_B}{2\hbar L}t \qquad \text{and} \qquad \phi_{12} = \phi_{21} = \frac{GM_AM_B}{\hbar\sqrt{4L^2 + (\Delta x)^2}}t. \tag{2.14}$$

Assuming again that the superposition size Δx is much smaller than the distance L between the masses - like before in eq. (2.2) - the phases $\phi_{12} = \phi_{21}$ can be expanded and a global phase ϕ can be factored:

$$\phi_{12} = \phi_{21} \approx \frac{GM_AM_B}{\hbar}\left[\frac{1}{2L} - \frac{(\Delta x)^2}{16L^3}\right]t \equiv \phi - \Delta\phi. \tag{2.15}$$

The state eq. (2.13) can now be expressed in the form

$$|\psi(t)\rangle = e^{i\phi}\frac{1}{\sqrt{2}}\left[\left|\psi_A^1\right\rangle \otimes \frac{|\psi_B^1\rangle + e^{-i\Delta\phi}\,|\psi_B^2\rangle}{\sqrt{2}} + \left|\psi_A^2\right\rangle \otimes \frac{e^{-i\Delta\phi}\,|\psi_B^1\rangle + |\psi_B^2\rangle}{\sqrt{2}}\right], \tag{2.16}$$

where the entanglement dynamics can be directly seen. This state is entangled, if it is not representable as a product state $|\psi\rangle \neq |\psi_A\rangle \otimes |\psi_B\rangle$. That is the case, if the states containing $|\psi_B^i\rangle$ are not both equal to each other (i.e. differ only by a phase) and thus cannot be factored. The system is therefore entangled, if and only if $\Delta\phi \neq k\pi$ with integer $k \in \mathbb{Z}$.

In order to assess in a more quantitative way how entangled the state $|\psi\rangle$ is, a more sophisticated entanglement measure is needed. In the next chapter, the ***logarithmic negativity*** is motivated and introduced. In the rest of this thesis, I will repeatedly opt for this measure.

2.2 Entanglement measures

Checking whether an arbitrary state ρ is entangled or not is no easy task. In fact, this problem is known to be NP-hard [14]. A state $\rho_{AB} \in \mathcal{H}_A \otimes \mathcal{H}_B$ is called entangled, if it is ***non-separable***, that is, it cannot be expressed as a tensor product of two subsystems $\rho_A \in \mathcal{H}_A$ and $\rho_B \in \mathcal{H}_B$. Only for specific cases - like the case of two qubits or qubit-qutrit - a simple sufficient criterion for determining the separability of a general mixed state is known: The positive partial transpose (PPT) criterion states, that if the partial transpose of the density matrix is positive ($\rho^{\Gamma_A} > 0$ [4]), the state ρ is separable [6, 7]. In other words, if ρ^{Γ_A} has negative eigenvalues, ρ is guaranteed to describe an entangled state. The inverse is true, if and only if the dimension of $\rho_A \otimes \rho_B$ is 2×2 or 3×2 [6] - otherwise, only having non-negative eigenvalues doesn't necessarily result in an unentangled system (such states are called "bound states"). The partial transpose with respect to a subsystem i can be understood in the same way as the partial trace, where the operation (in this case the transform) is performed only on indices corresponding the subsystem ρ_i. To see the necessity of the PPT criterion, consider a separable mixed state ρ, which can be generally expressed as

$$\rho = \sum p_i \rho_A^i \otimes \rho_B^i. \tag{2.17}$$

The partial transpose is in this case trivial:

$$\rho^{\Gamma_A} = \sum p_i (\rho_A^i)^T \otimes \rho_B^i. \tag{2.18}$$

Since the transpose preserves eigenvalues, the transposed subsystem A is still positive $(\rho_A^i)^T > 0$ and describes again a valid quantum state. It follows, that ρ^{Γ_A} is positive as well. If somehow ρ^{Γ_A} has any negative eigenvalues, this can only mean that the initial

[4] A matrix is defined as positive ("positive definite"), if all eigenvalues are positive.

state ρ is not separable and cannot be expressed in the form of eq. (2.17) and the necessity of the criterion is shown.

For quantifying entanglement in a more precise way, a mathematical quantity called ***entanglement measure*** can be used. A good measure should be able to capture the essential features of entanglement. One can axiomatically state what properties such a measure $E(\rho)$ should have [6, 7]:

Normalization An entanglement measure should be a mapping from densities to real positive values between 0 and 1:

$$\rho \to E(\rho) \in \mathbb{R}^+ \tag{2.19}$$

where usually the maximally entangled state has $E = 1$.

Monotonicity under LOCC E should not increase under local operations and classical communications. This is the most important postulate for an entanglement measure and often cited as the *only* required postulate.

Vanishing on separable states $E(\rho) = 0$ if ρ is separable

Often one finds additional properties useful like *convexity* $E(\sum p_i\rho_i) \leq \sum p_i E(\rho_i)$ or (full) *additivity* $E(\rho \otimes \sigma) = E(\rho) + E(\sigma)$.

A function that satisfies the most important of these conditions is often called an *entanglement monotone*.

The ***negativity*** $\mathcal{N}$ is such an entanglement monotone [7, 15] that used the PPT criterion to determine if a state is entangled or not. It is defined as

$$\mathcal{N} = \frac{\left\|\rho^{\Gamma_A}\right\|_1 - 1}{2} \tag{2.20}$$

where $\|A\|_1 = \operatorname{tr}|A| = \operatorname{tr}\sqrt{A^\dagger A}$ is the trace norm. The negativity however is not additive and a more suitable and widely used entanglement measure is the ***logarithmic negativity*** [6, 7, 16]

$$E_N(\rho) = \log_2 \left\|\rho^{\Gamma_A}\right\|_1 . \tag{2.21}$$

The monotonicity of the logarithm implies, that E_N is an entanglement monotone as well. Furthermore, for the calculations it does not matter which subsystem is transposed.

Proposition 2.2. *a) The partial transpose w.r.t. subsystem A is equal to the transposed partial transpose w.r.t. subsystem B:* $\rho^{\Gamma_A} = (\rho^{\Gamma_B})^T$. *b) The trace norms of partially transposed density operators w.r.t. any subsystem are equal:* $\left\|\rho^{\Gamma_A}\right\|_1 = \left\|\rho^{\Gamma_B}\right\|_1$.

Proof. a) A general density matrix ρ can be expressed as

$$\rho = \sum_{i,j,k,l} \rho_{ij,kl} \, |i\rangle\langle j|_A \otimes |k\rangle\langle l|_B$$

The partial transpose with respect to subsystem B is then defined as

$$\rho^{\Gamma_B} \equiv \sum_{i,j,k,l} \rho_{ij,kl} \left|i\right\rangle\!\left\langle j\right|_A \otimes \left(\left|k\right\rangle\!\left\langle l\right|_B\right)^T = \sum_{i,j,k,l} c_{ij,kl} \left|i\right\rangle\!\left\langle j\right|_A \otimes \left|l\right\rangle\!\left\langle k\right|_B$$

The complete transpose of this is

$$(\rho^{\Gamma_B})^T = \sum_{i,j,k,l} \rho_{ij,kl} \left(\left|i\right\rangle\!\left\langle j\right|_A\right)^T \otimes \left(\left|l\right\rangle\!\left\langle k\right|_B\right)^T = \sum_{i,j,k,l} c_{ij,kl} \left|j\right\rangle\!\left\langle i\right|_A \otimes \left|k\right\rangle\!\left\langle l\right|_B \equiv \rho^{\Gamma_A}$$

b) Clear by a) and by using lemma 2.1 and the fact that the eigenvalues of a square matrix A and A^T are equal. □

The logarithmic negativity is very easy to calculate compared to other entanglement measures. It is enough to compute the square root of the eigenvalues of $(\rho^\Gamma)^\dagger\rho^\Gamma$ or the absolute sum of the eigenvalues of ρ^Γ. For practical and numeric calculations it is often more easy and stable to take a single eigenvalue than the need to compute the sum of multiple. For all numerical calculations in this thesis, I therefore opt for an alternative way to compute the logarithmic negativity.

Lemma 2.1. *The trace norm $\|A\|_1 \equiv \operatorname{tr}\sqrt{A^\dagger A}$ of a hermitian matrix A is equal to the sum of the absolute eigenvalues of A.*

Proof. This can be immediately seen by the spectral theorem:

$$\operatorname{tr}\sqrt{A^\dagger A} = \operatorname{tr}\sqrt{A^2} = \operatorname{tr}\left\{U\sqrt{\operatorname{diag}(\lambda_1,\dots)^2}U^\dagger\right\} = \sum_i \sqrt{\lambda_i^2} = \sum_i |\lambda_i| \,.$$

□

Proposition 2.3. *The negativity eq.* (2.20) *is given as the absolute sum of all negative eigenvalues of ρ^Γ:*

$$\mathscr{N}(\rho) \equiv \frac{\left\|\rho^\Gamma\right\|_1 - 1}{2} = \left|\sum_{\lambda_i<0} \lambda_i\right| . \tag{2.22}$$

Proof. The proof is in parts given by Vidal and Werner [15]. It is known that the density matrix is hermitian: $\rho = \rho^\dagger$. Using lemma 2.1, the trace norm of the density matrix is is given as $\|\rho\|_1 = \sum\lambda_i = \operatorname{tr}\rho = 1$. The partial transpose ρ^Γ obviously also satisfies $\operatorname{tr}\rho^\Gamma = 1$ but might have negative eigenvalues. Since ρ^Γ is still hermitian, the trace norm is given by

$$\left\|\rho^\Gamma\right\|_1 = \sum_i |\lambda_i| = \sum_{\lambda_i\geq 0} \lambda_i + \sum_{\lambda_i<0} |\lambda_i| = \sum_i \lambda_i + 2\sum_{\lambda_i<0} |\lambda_i| = 1 + 2\sum_{\lambda_i<0} |\lambda_i| \,,$$

where in the last step $\sum\lambda_i = \operatorname{tr}\rho^\Gamma = 1$ was used. The negativity can be defined as $\mathscr{N}(\rho) = \left|\sum_{\lambda_i<0}\lambda_i\right|$ and the statement is shown. □

Remark. The PPT criterion states, that if ρ^Γ has negative eigenvalues, the state ρ is entangled. The negativity uses this criterion for a quantification of entanglement. This proposition makes sense of the name *negativity*.

Calculating the logarithmic negativity of the evolved state eq. (2.13), it is possible to quantify how the entanglement behaves in time. A straight forward computation following the calculation methods established above yields (for detailed calculations see appendix A.2)

$$E_N(|\psi(t)\rangle\langle\psi(t)|) = \log_2\left(1 + |\sin\Delta\phi|\right). \tag{2.23}$$

It is interesting to see, that the maximum entanglement $E_N = 1$ is reached for $\Delta\phi = 2\pi k \pm \pi/2$, $k \in \mathbb{Z}$ and no entanglement ($E_N = 0$) is measurable for $\Delta\phi = k\pi$. This result aligns with the previous observations by demanding that the evolved state eq. (2.13) is separable. The complete entanglement dynamics are shown in fig. 2.2. The time

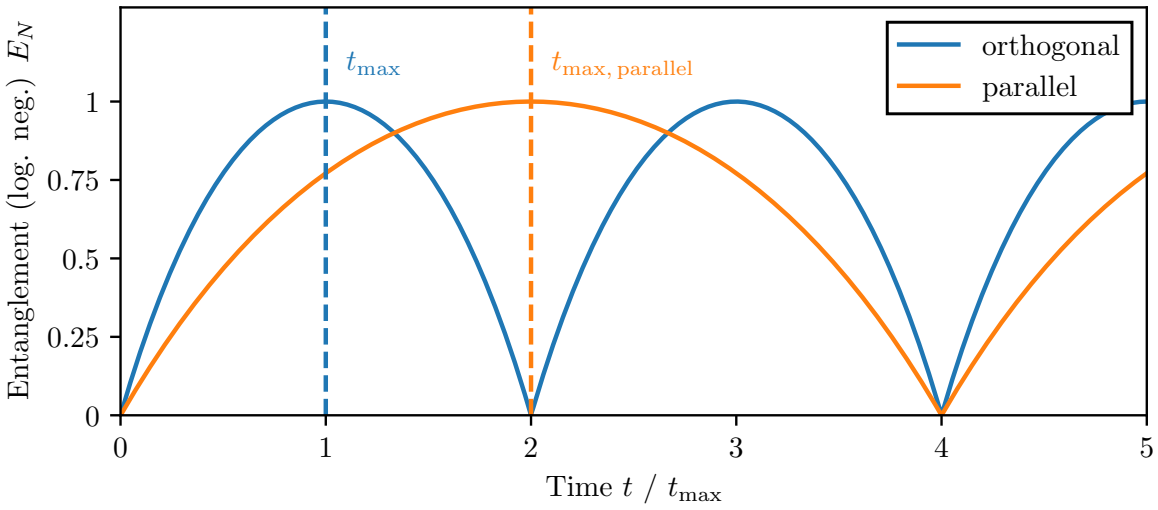

Figure 2.2: Entanglement dynamics quantified by the logarithmic negativity for two different orientations of the spatial superpositions. The parallel orientation was considered in this chapter (see eq. (2.23)), the "orhtogonal" one in Ref. [8]. The time of maximum entanglement $t_{\max}$ for the orthogonal configuration is reached after $t_{\max} = 4\pi\hbar L^3/(GM_AM_B\Delta x^2) \simeq 129\,\text{ms}$.

$t_{\max,\,\text{parallel}}$ at which the entanglement is maximal (for the first time) can be calculated by using the definition of $\Delta\phi$ from eq. (2.15) as

$$t_{\max,\,\text{parallel}} = \frac{8\pi L^3\hbar}{GM_AM_B(\Delta x)^2}. \tag{2.24}$$

In fig. 2.2 the entanglement dynamics for a different orientation considered in Ref. [8] is also shown. There, the superpositions are aligned in the same line as the direct connection between the masses ("orthogonal" to the parallel configuration before), maximizing the differences in distances between them and thus creating entanglement faster. This

expected behavior can be well seen in fig. 2.2: The time $t_{\max}$ until the maximum entanglement is reached, is precisely by a factor of 2 faster than in the here considered parallel configuration [8]. For a practical experiment, this suggests that using the orthogonal orientation could be beneficial and would require shorter coherence times for the superpositions. To give an estimate, consider two identical silica spheres with a density of $\rho = 2648\,\mathrm{kg/m^3}$ with a radius of $R = 10^{-5}\,\mathrm{m}$, a separation of $2L = 4R$ and a superposition size $\Delta x = 100\,\mathrm{nm}$ (which is realistic considering theoretical sizes of up to micrometers [4]), the maximum entanglement is reached after about $t_{\max} \approx 129\,\mathrm{ms}$ which is a quite long coherence time and challenging experimentally.

2.3 Issues with the experimental procedure

Additional effects: - Casimir forces entangle as well - Coulomb forces

-¿ solution: conducting faraday shield, UV discharge [17]

How to measure? Many measurements are necessary -¿ Entanglement witness? Measure density directly -¿ Small variations for each measurement in angle of the superposition and in distance to the newly introduced shield

3 Casimir effect

Casimir forces can be viewed in a very similar way to the *van der Waals forces*. In fact, both phenomena describe just two different sides of the same coin. They define the so-called ***dispersion forces*** between neutral atoms or bodies. The quantum theory of van der Waals forces between two neutral atoms was developed by London in 1930 who found the attractive potential $\propto 1/r^6$ for small separations [18]. Casimir and Polder showed in 1948, that for separations larger than the resonance wavelength of the atoms, retardation effects need to be taken into account and the potential decays by a power law of $1/r^7$ [13]. Additionally, they calculated the interaction with a atom or molecule and a perfectly conducting wall, showing that macroscopic objects could experience these ***Casimir-Polder interactions*** as well. It becomes evident, that a full description of dispersion forces cannot be given by classical electrodynamics alone. Additional considerations regarding relativistic effects and quantum electrodynamics have to be made [19–21]. Casimir, following a suggestion by Bohr [22], found a simple derivation using the zero-point energy of the vacuum to calculate the attraction between two conducting plates. In quantum electrodynamics each point in the electromagnetic field can be described by an quantized harmonic oscillator with ground state energy $E_0 = \hbar\omega/2$. The total *zero-point energy* of the ground state of the field (the vacuum) is therefore given by summing over the energies E_0 for each possible mode n

$$E_{\text{vacuum}} = \frac{\hbar}{2}\sum_n \omega_n. \tag{3.1}$$

These sums are clearly divergent since there are infinitely many possible excitations. Electrostatic boundary conditions require the field to be zero at the surface of the plate restricting the possible modes between the plates. Precisely the finite difference between the infinite vacuum energy with and without the plates give rise to the ***Casimir forces*** between two macroscopic objects. A lot of textbooks are simply dropping the divergence motivated by the fact that energy is normally defined only up to a constant [19]. Casimir was able to use regularization techniques to deal with the infinite quantities and arrived at his famous formula [12]

$$E_{\text{Casimir}} = -\frac{\hbar c\pi^2}{720L^3}A. \tag{3.2}$$

for the attractive Casimir-potential between two plates with area A and separation L. The attractive force between the plates can now be simply expressed as

$$F_{\text{Casimir}} = -\frac{\hbar c\pi^2}{240L^4}A. \tag{3.3}$$

It is remarkable, that such a simple relation arises out of the infinities of the vacuum. Up until now, these Casimir forces are topic of modern scientific research. They are generally very difficult to calculate for other geometries than two infinitely large plates or for real materials with dielectric properties. Even for simple geometries, even the sign of the force is not always intuitively clear: As an example, the Casimir force can be repulsive for an ideal metal spherical shell [20]. For other simple and important bodies like the sphere-plane or sphere-sphere geometry, no universally valid formula for any separation between the bodies exists. This is discussed in more detail in section 3.2.

Almost ten years after the discovery of Casimir and Polder, Lifshitz was the first to find an expression for the Casimir force between two dielectric plates with arbitrary relative permittivity $\varepsilon_{r,1,2}$ for separations larger than the resonant wavelength [5] [24]. The expression he found facilitates the general complexity of the Casimir interactions and is only expressible as a complicated integral [24]

$$F/A = -\frac{\hbar c}{32\pi^2 L^4}\int_0^\infty \mathrm{d}x \int_1^\infty \mathrm{d}p\ \frac{x^3}{p^2}\left\{\left[\frac{(s_1+p)(s_2+p)}{(s_1-p)(s_2-p)}e^x - 1\right]^{-1} + \left[\frac{(s_1+\varepsilon_{r,1}p)(s_2+\varepsilon_{r,2}p)}{(s_1-\varepsilon_{r,1}p)(s_2-\varepsilon_{r,2}p)}e^x - 1\right]^{-1}\right\} \quad (3.4)$$

with

$$s_{1,2} = \sqrt{\varepsilon_{r,1,2} - 1 + p^2}.$$

In the limit of two perfectly conducting plates ($\varepsilon_{r,1} = \varepsilon_{r,2} \to \infty$), the integral can be solved analytically and one gets the same expression already obtained by Casimir

$$F_{\text{cond.}}/A = -\frac{\hbar c}{16\pi^2 L^4}\int_0^\infty \mathrm{d}x \int_1^\infty \mathrm{d}p\ \frac{x^3}{p^2(e^x-1)} = -\frac{\hbar c \pi^2}{240 L^4}. \quad (3.5)$$

Lifshitz determined the Casimir force between a conducting metal plate and a dielectric plate (denoted DM) as well as the force between two dielectric plates with the same dielectric constant ε_r (DD) as

$$F_{\text{DM}} = -\frac{\hbar c \pi^2}{240 L^4}\frac{\varepsilon_r - 1}{\varepsilon_r + 1}\varphi(\varepsilon_r) \quad (3.6)$$

$$F_{\text{DD}} = -\frac{\hbar c \pi^2}{240 L^4}\left(\frac{\varepsilon_r - 1}{\varepsilon_r + 1}\right)^2 \varphi(\varepsilon_r) \quad (3.7)$$

where $\varphi(\varepsilon_r)$ is a numerical function obtained by solving eq. (3.4), which approaches 1 for a perfect conductor. I calculated the function numerically and the result is shown in fig. 3.1. For a dielectric and metal plate, the function φ approaches the finite value $\varphi(\varepsilon_r \to 1) \approx 0.46$ for small dielectric constants. However, this limit is practically already reached at $\varepsilon_r \approx 4$ and φ stays approximately constant for smaller ε_r.

[5] The "resonance wavelength" for a macroscopic body in this case can be understood as e.g. the plasma frequency in the Drude model [23]. Different models for light-matter interaction result in slightly different resonant wavelength. The Lifshitz formula however holds true for the cases of separations in the micro-meter regime for all practical materials [17].

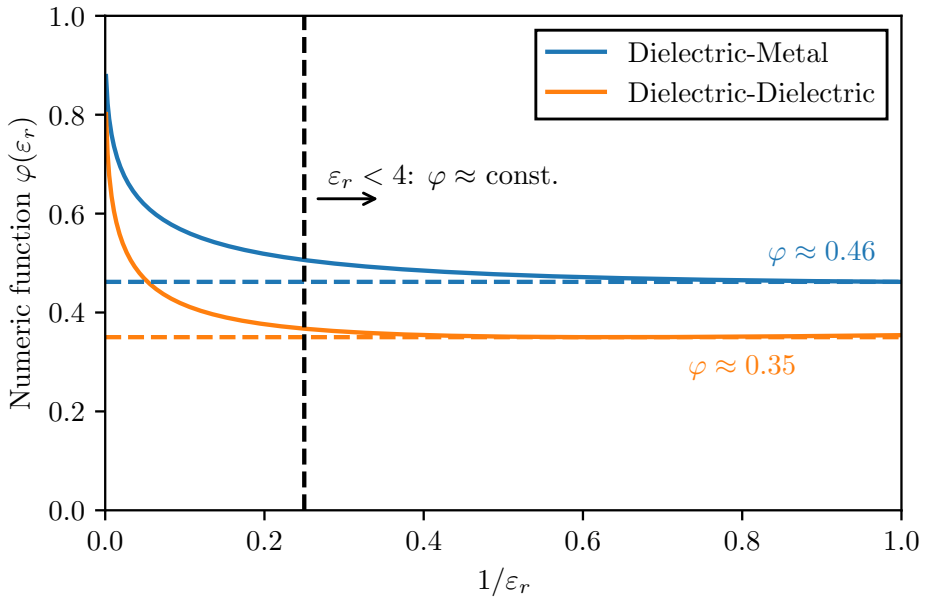

Figure 3.1: Numeric calculations of the function $\varphi(\varepsilon)$ used in the Lifshitz formula eq. (3.6) and (3.7). The function was calculated for **(blue)** a dielectric and a metal plates and **(orange)** two dielectric plates. The function approaches unity for $\varepsilon \to \infty$ and a finite value for $\varepsilon \to 1$.

3.1 Proximity force approximation

The Casimir-Polder force cannot be computed easily for different shapes. There even exists no analytic expression for the simple (and for this thesis relevant) plate-sphere geometry for all ratios L/R and plate-sphere separations. For a general shape, even the sign of the force, i.e. whether it is attractive or repulsive, is often unknown. Fortunately, approximation methods exist and in particular the ***proximity-force-approximation (PFA)*** can be calculated very easily [25–27]. The PFA is only valid for small separations ($L/R \approx 1$) between the considered smooth bodies. The idea of this approximation is to divide the surfaces of the two bodies into infinitesimal small parallel plates with area $\mathrm{d}A$ and summing over the forces $\mathrm{d}F$ (or the Casimir-energy $\mathrm{d}E$) between them (see fig. 3.2):

$$E_{\mathrm{PFA}} = \iint_A \mathrm{d}A \, \frac{E_{\mathrm{plate-plate}}}{A} \tag{3.8}$$

where for the casimir energy per unit area $E_{\mathrm{plate-plate}}/A$ either eq. (3.2) or any of the Lifshitz equations (3.7), (3.6) can be chosen. For the following calculations, it is important to distinguish between the distance between the plates center and the spheres center L (like used before) and the edge-to-edge distance $\mathscr{L} = L - R$.

The problem with this approximation is, that it is ambiguous, what surface the area element $\mathrm{d}A$ represents. For the plate-sphere geometry, the element can be either chosen tangential to the sphere or parallel to the plate (or in theory any other fictitious surface

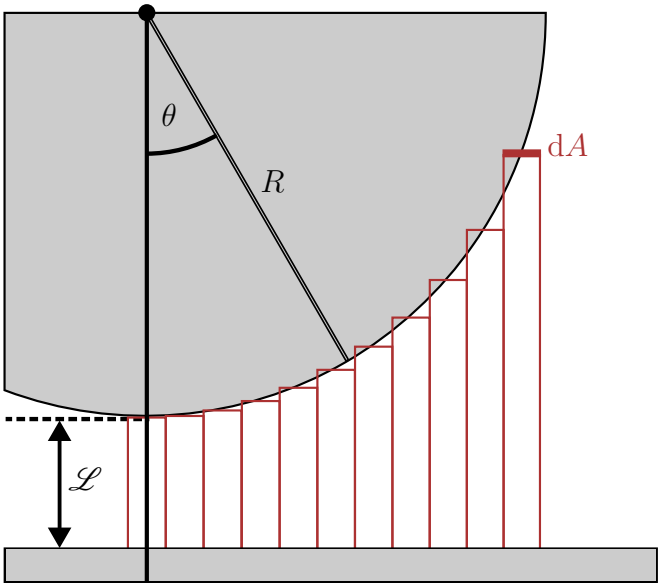

Figure 3.2: In the proximity force approximation the sphere is divided into infinitesimal plane areas $\mathrm{d}A$ which all exert a force $\mathrm{d}F$ according to eq. (3.3). All the contributions are added up together.

somewhere in between) [27]. For the plate-sphere geometry, in the limit of the validity of the PFA $\mathscr{L} \ll R$ both methods yield the same result. For the following calculations, I choose $\mathrm{d}A$ parallel to the plate and the area can be parameterized with $r \in [0, R]$ and $\varphi \in [0, 2\pi]$ resulting in a distance z between the infinitesimal area elements $z(r) = \mathscr{L} + R - \sqrt{R^2 - r^2}$ [6]. The PFA eq. (3.8) then yields for a dielectric sphere against a perfectly conducting plate

$$E_{\text{plate-sphere}} = -\frac{\hbar c \pi^2}{720}\left(\frac{\varepsilon_r - 1}{\varepsilon_r + 1}\right)\varphi(\varepsilon_r)\int_0^R \mathrm{d}r \int_0^{2\pi} r\mathrm{d}\varphi \frac{1}{z(r)^3} \tag{3.9}$$

$$= -\frac{\hbar c \pi^3}{360}\left(\frac{\varepsilon_r - 1}{\varepsilon_r + 1}\right)\varphi(\varepsilon_r)\frac{R^2}{2\mathscr{L}^2(R + \mathscr{L})} \tag{3.10}$$

$$\approx -\frac{\hbar c \pi^3}{720}\left(\frac{\varepsilon_r - 1}{\varepsilon_r + 1}\right)\varphi(\varepsilon_r)\frac{R}{\mathscr{L}^2} \tag{3.11}$$

3.2 Casimir forces between a conducting plate and a dielectric sphere

An empirical derivation for power law of the casimir energy between a sphere and a conducting plate can be made directly from the energy between two atoms with static

[6] Taking $\mathrm{d}A$ tangential to the sphere, it can be parameterized with $\theta \in [0, \pi/2]$ and $\varphi \in [0, 2\pi]$ resulting in $z(\theta) = \mathscr{L} + R - R\cos\theta$. The PFA eq. (3.8) yields with $\mathrm{d}A = R^2 \sin\theta \mathrm{d}\theta\mathrm{d}\varphi$ the result $\propto \frac{\pi R^2(R+2\mathscr{L})}{\mathscr{L}^2(R+\mathscr{L})^2}$ which in the limit of $\mathscr{L} \ll R$ results in the same expression as eq. (3.11).

polarizability α_i given by Casimir and Polder [13]. They derived an expression for the Casimir-Polder potential of [7]

$$E = -\frac{23\hbar c \alpha_1 \alpha_2}{4\pi L^7}. \tag{3.12}$$

The polarizability of a sphere with radius R is derived in appendix B.1 and is given for an dielectric with ε_r as

$$\alpha_{\text{sphere}} = \left(\frac{\varepsilon_r - 1}{\varepsilon_r + 2}\right) R^3. \tag{3.13}$$

If one atom is now replaced by a conducting sphere ($\varepsilon_r \to 1$) of radius $\sim L$ (much larger than the atom) with a polarizability of L^3, it get obvious that between this big sphere and the atom, the energy is given by a power law of $1/L^4$. It is therefore natural to assume, that for a macroscopic sphere and a macroscopic plate, the Casimir energy behaves similar to a $1/L^4$ law - at least for the *large separation limit* (LSL). The exact calculation for this problem is very hard. In fact, no analytic solution is known.

Ford was able to determine an integral expression using a macroscopic approach in 1998 [23]:

$$F = -\frac{\hbar c}{4\pi L^4} \int_0^\infty \mathrm{d}\omega\, \alpha(\omega) \left[3 \sin 2\omega L - 6L\omega \cos 2\omega L \right. \\ \left. -6L^2\omega^2 \sin 2\omega L + 4L^3\omega^3 \cos 2\omega L\right]. \tag{3.14}$$

The expression depends on the polarizability, which is generally not constant for a dielectric. Especially for small separations between the sphere and the plate, this dependence and the non-constant polarizability make this integral nearly unsolvable. For large separations, much larger than the absorption wavelength of the dielectric or much larger than the wavelength corresponding to the plasma frequency in the Drude-Model, the polarizability can be assumed to be static $\alpha = \text{const}$ [17, 23]. In this simplifying case, the integral can be solved using an exponential convergence factor and results in

$$F = -\frac{6\hbar c}{4\pi L^5} \alpha \tag{3.15}$$

and thus

$$E = -\frac{3}{8} \frac{\hbar c}{\pi L^4} \left(\frac{\varepsilon_r - 1}{\varepsilon_r + 2}\right) R^3. \tag{3.16}$$

For the large separation limit, the Casimir interaction between a sphere and a plate behaves like expected considering the motivation of the $1/L^4$-law above in this section.

- Series expansion

- Comparison to PFA

- Showing PFA is always the maximum

[7] For two macroscopic spheres, the casimir potential looks very similar to eq. (3.12). The polarizability of a sphere is given by eq. (3.13). Using this result, the Casimir energy between two identical dielectric spheres is given as $-\frac{23\hbar c}{4\pi L^7} \left(\frac{\varepsilon_r - 1}{\varepsilon_r + 2}\right)^2 R^6$. !!!CITATION!!!

Theorem 3.1. *The PFA model predicts a stronger casimir potential for all separations L/R than the LSL or the exact series expansion.*

Proof. a) Series expansion in the one paper. $LSL/PFA \leq 1$ for all L/R [26].

b) Better than LSL (proof) □

Remark. This is rather unintuitive, because one would expect it to be the other way around. The $1/L^4$ dependence in the LSL should - for small separations - tend much faster to zero than the $1/\mathscr{L}^2$ dependence in the PFA. However considering the differences between L and $\mathscr{L} = L - R$, this is no longer surprising.

3.3 Imperfect plate and spheres

Python numerical approach, gaussian modes (vibration modes of a spherical plane), perlin noise

4 The shield

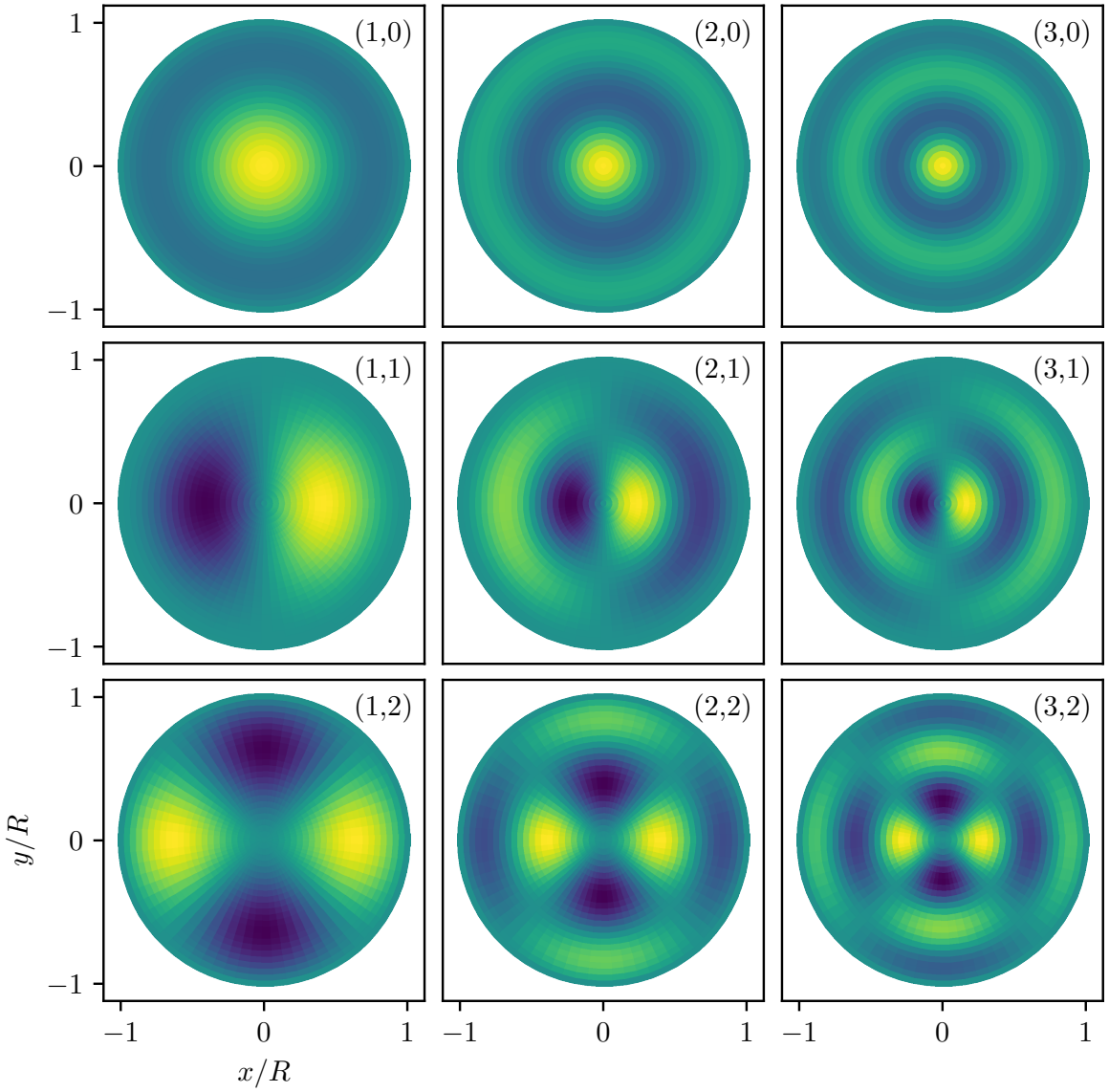

Figure 4.1: Vibrational modes of a spherical plate fixed at the edge with $R/d = 1000$.

The modes (k,l), $1 \leq k$, $0 \leq l$ have the shape

$$u_{kl}(r,\theta,t) = A\left[J_l(\sqrt{\beta_k}r) - \frac{J_l(\sqrt{\beta_k}r_s)}{I_l(\sqrt{\beta_k}r_s)} I_l(\sqrt{\beta_k}r)\right]\cos(l\theta+\phi_1)\sin(\omega_{kl}t+\phi_2) \tag{4.1}$$

with

$$\beta_k = \frac{\tilde{r}_k^2}{r_s^2} \qquad \omega_{kl} = \frac{\tilde{r}_k^2}{r_s^2}\sqrt{\frac{D}{\rho d}} = \tilde{x}_l^2 \frac{d}{r_s^2}\sqrt{\frac{E}{12\rho(1-\nu^2)}}, \tag{4.2}$$

where $\tilde{r}_k$ is the k-th solution of the equation

$$J_l(\tilde{r}_k)I_{l+1}(\tilde{r}_k) + I_l(\tilde{r}_k)J_{l+1}(\tilde{r}_k) = 0. \tag{4.3}$$

4.1 Occupation of the modes

Because of the modes u_{kl}, both superposition states of delocalized cat-state in front of the shield are effected by a slightly different Casimir-force. This force depends on the surface-to-surface distance $\mathscr{L}$ between the shield and the mass. This distance changes slightly due to the thermal motion of the shield by a difference of $A \cdot u_{k,l}(r_{\text{pos}})$ where r_{pos} is the position of the particle. During time evolution, a slightly different phase is introduced for the two delocalized states. I am interested, which modes matters the most and introduce the most dephasing in a parallel superposition in front of the shield. This information is useful for a worst-case estimate on how much angular and distance fluctuations in the positioning of the particle are introduced through thermal effects. Experimentally, one therefore needs to find a regime in which entanglement can still be measured regardless of these thermal vibrations.

Assuming a shield made out of copper with $\rho = 8960\,\text{kg/m}^3$, $E = 110\,\text{GPa}$ and $\nu = 1/3$, the vibrational frequencies for a thin shield ($d = 100\,\text{nm}$ and $r_s = 0.01\,\text{m}$) are given in the order of $\omega_{1,0} = 11.0\,\text{s}^{-1}$ up to $\omega_{10,11} = 3108.9\,\text{s}^{-1}$. Because of these low frequencies, the energy $\hbar\omega$ of the mode vibrations are much smaller than the thermal energy $k_B T$ for a reasonable temperature. This means, that all modes are approximately occupied uniformly. The amplitude z of each mode of the plate vibrations can be thought of as an quantum harmonic oscillator with frequency ω_{kl}. At a temperature T, the expected amplitude is given by $\langle z_{kl}\rangle = 0$ with a variance of (a derivation is given in appendix C.1)

$$\left\langle z_{kl}^2 \right\rangle_T = \frac{\hbar}{2\tilde{m}\omega_{kl}} \coth\left(\frac{\hbar\omega_{kl}}{2k_B T}\right) \approx \frac{k_B T}{\tilde{m}\omega_{kl}^2} \tag{4.4}$$

where in the last step $\hbar\omega \ll k_B T$ was used. $\tilde{m}$ is the *effective mass* of the mode in which the precise shape is considered. A intuitive estimation for this mass can be given by the average of the mode

$$\tilde{m} = m\frac{1}{\pi r_s^2}\int_0^{r_s} \mathrm{d}r \int_0^{2\pi} r\mathrm{d}\theta\, u_{kl}(r,\theta,t). \tag{4.5}$$

with $m = \rho\pi r_s^2 d$ being the total mass of the shield. Due to the high occupation number of oscillator modes, the probability $p(z)$ of finding an oscillation with amplitude z is approximately a gaussian normal distribution around $\langle z_{kl}\rangle = 0$ with the standard deviation given by the square-root of $(\Delta z_{kl})_T^2 = \langle z_{kl}^2\rangle_T - \langle z_{kl}\rangle$. Luckily it seems that the on average, the standard deviation decreases with $1/\omega$ which means, that higher-order modes with larger frequencies are still highly occupied but should contribute less to the total vibration. To quantify this, I considered the dephasing of a single parallel delocalized cat-state in front of the plate. The phase difference $\Delta\phi$ is given by

$$\Delta\phi(z) = \frac{t}{\hbar}\frac{\hbar c\pi^3}{720}R\left[\frac{1}{(\mathscr{L} - z\cdot u_{kl}(r-\Delta x/2))^2} - \frac{1}{(\mathscr{L} - z\cdot u_{kl}(r+\Delta x/2))^2}\right] \tag{4.6}$$

when the particle is placed at a distance r from the center of the plate. In the following the two cases are considered, where the particle is placed in the center at $r = 0$ and in the worst-case position of mode $(1,0)$, where the gradient is maximized ($r \approx 0.5274 r_s$). The dephasing rate γ is now given by

$$e^{-\gamma} = \left\langle e^{-i\Delta\phi}\right\rangle = \int_{-\infty}^{\infty} \mathrm{d}z\, \frac{1}{\sqrt{2\pi(\Delta z_{kl})_T^2}} \exp\left\{-\frac{z^2}{2(\Delta z_{kl})_T^2}\right\} e^{-i\Delta\phi(z)}. \tag{4.7}$$

In fig. 4.2 the dephasing γ is shown. The non-trivial behavior arises because of the

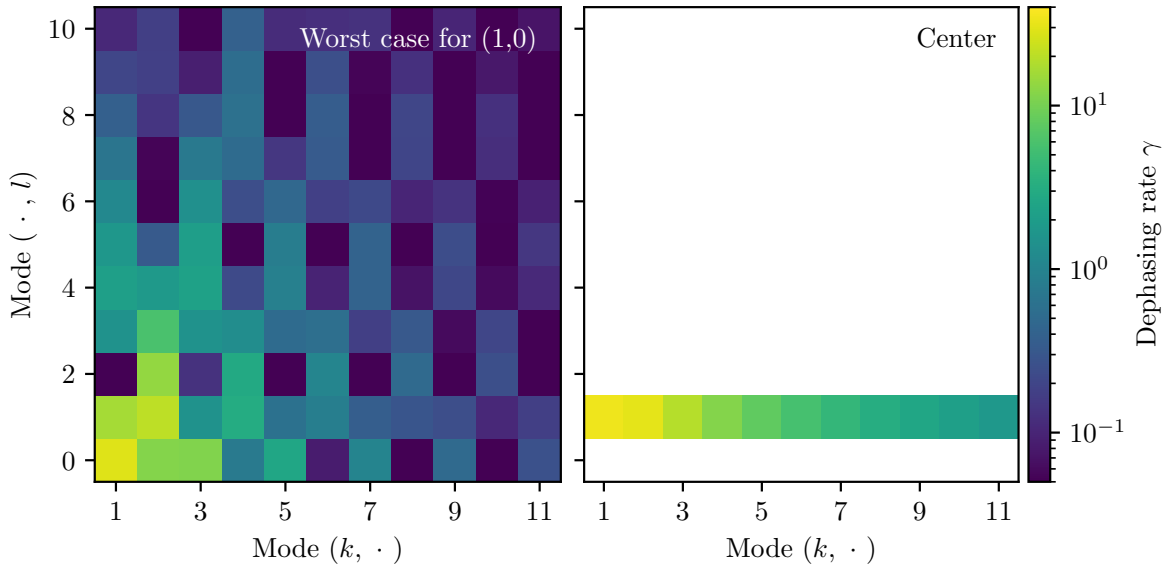

Figure 4.2: Dephasing rate γ of a delocalized cat-state positioned parallel to the shield at $T = 4\,\mathrm{K}$. **left:** the worst-case estimate where the state is placed in the point with the maximum gradient ($r \approx 0.5274 r_s$). **right:** realistic scenario with the cat-state placed at the center.

different mode-shapes. Nevertheless, a clear trend is observable where all highly excited

modes don't contribute to the dephasing. Assuming, that the amplitude z is much smaller than $\mathscr{L}$ [8], the phase-difference eq. (4.6) can be expanded to

$$\Delta\phi(z) \approx \frac{c\pi^3 Rt}{720} \cdot \frac{2\left(u_{kl}(r-\Delta x/2) - u_{kl}(r+\Delta x/2)\right) z}{\mathscr{L}^3} \equiv gz \tag{4.8}$$

Averaging over z using again the probability distribution $p(z)$ like in eq. (4.7), the resulting expression is given by

$$e^{-\gamma} \approx \int_{-\infty}^{\infty} \mathrm{d}z\, p(z) e^{-igz} = \exp\left\{-\frac{g^2(\Delta z_{kl})_T^2}{2}\right\} \approx \exp\left\{-\frac{\Delta\phi^2\left(\sqrt{(\Delta z_{kl})_T^2}\right)}{2}\right\}. \tag{4.9}$$

It is therefore enough for further calculations, to actually use the thermal variance of the oscillator $(\Delta z_{kl})_T^2$ for the amplitude for all modes. The error done by this approximation is shown in fig. 4.3. Furthermore, the numerical results in fig. 4.2 suggest that only very

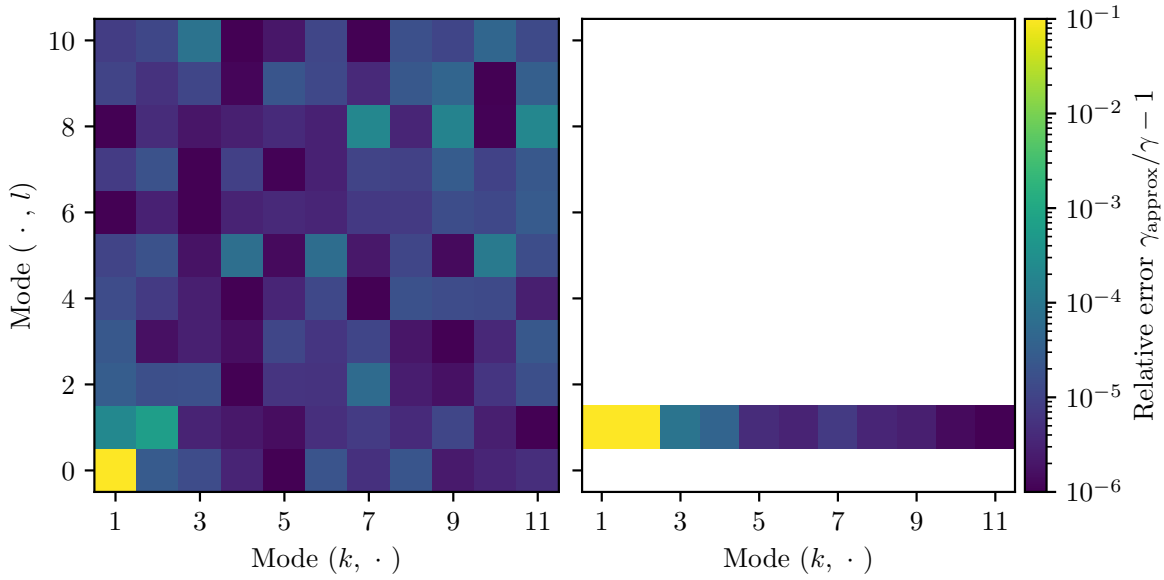

Figure 4.3: Relative error $|\gamma_{\mathrm{approx}}/\gamma - 1|$ by using $\gamma_{\mathrm{approx}} = \Delta\phi^2\left(\sqrt{(\Delta z_{kl})_T^2}\right)/2$. Hardly any notable error is therefore made by these approximations for higher order modes. The approximation only overestimates the lowest modes by a factor of ~ 3.

low modes need to be taken into account for all further considerations.

[8] Which is true, considering that $\sqrt{(\Delta z_{1,0}^2)_T} \approx 1.807 \times 10^{-9}\,\mathrm{m}$ compared to $\mathscr{L} \approx R \sim 10^{-6}\,\mathrm{m}$.

4.2 Effects of the modes

The amplitude A of the vibrational mode (k, l) is given by $A \sim \sqrt{(\Delta z_{kl})_T^2}$ where $(\Delta z)^2 = \langle z^2 \rangle - \langle z \rangle^2$ is the variance of the oscillator mode

$$(\Delta z_{kl})_T^2 = \frac{\hbar}{2\tilde{m}\omega_{kl}} \coth\left(\frac{\hbar\omega_{kl}}{2k_B T}\right). \tag{4.10}$$

Shield vibrations can be understood like

$$\alpha = \beta = \arctan \max_{\substack{0\le r\le r_s \\ \theta\in[0,2\pi) \\ t\in[0,2\pi/\omega_{kl})}} \left|\frac{\partial}{\partial r} u_{kl}(r,\theta,t)\right| \tag{4.11}$$

and

$$\Delta L = u_{kl}\left(\operatorname*{argmax}_{\substack{0\le r\le r_s \\ \theta,t}} \left|\frac{\partial}{\partial r} u_{kl}\right|\right) \lesssim \sqrt{\langle x_{kl}^2 \rangle_T} \tag{4.12}$$

$$\approx \frac{1}{r_s}\left(r_s - \operatorname*{argmax}_{0\le r\le r_s} \left|\frac{\partial}{\partial r} u_{kl}\right|\right) \sqrt{\langle x_{kl}^2 \rangle_T} \tag{4.13}$$

5 The optimal setup

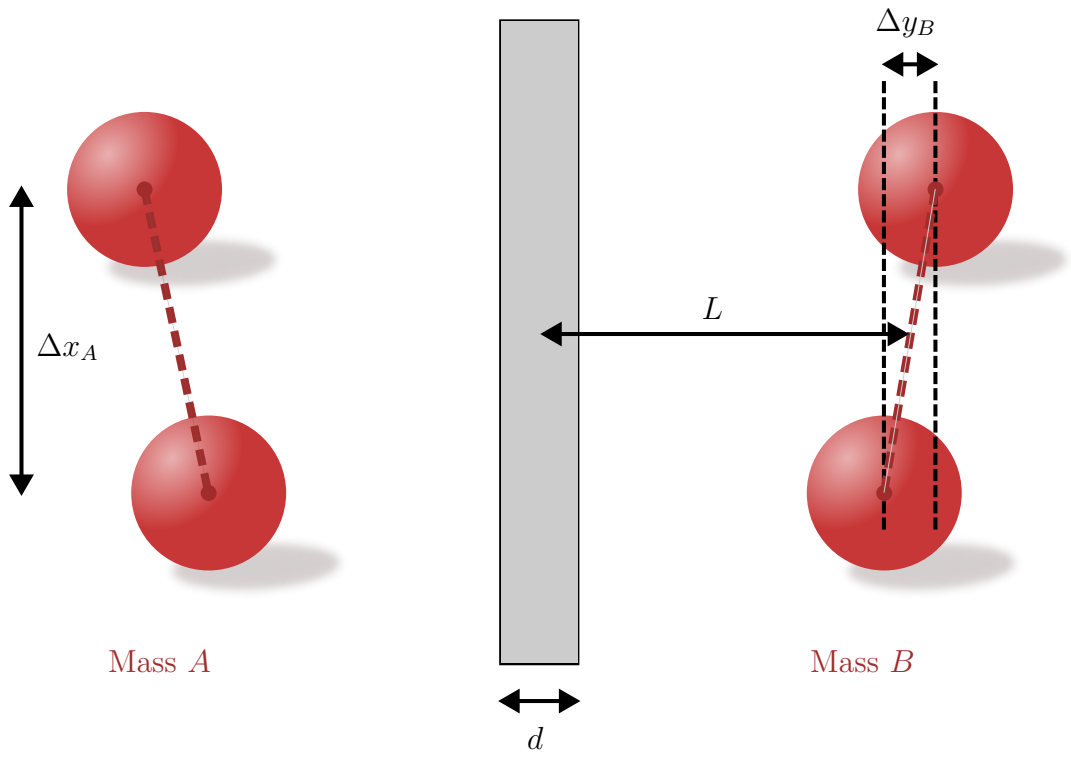

Figure 5.1: My problem

5.1 Orientation

E_N depending on the orientation:

$$E_N = \log_2 \left\{ 1 + \left| \sin\left(\frac{GM_A M_B t}{\hbar} \frac{\Delta x_A \Delta x_B}{8L^3} \left[\sin\alpha \sin\beta - \frac{1}{2} \cos\alpha \cos\beta \right] \right) \right| \right\} \tag{5.1}$$

Time till the maximum entanglement ($E_N = 1$):

$$t_{\max} = \frac{8\pi L^3 \hbar}{2GM_A M_B \Delta x_A \Delta x_B} \left| \sin\alpha \sin\beta - \frac{1}{2} \cos\alpha \cos\beta \right|^{-1} \tag{5.2}$$

with a global minimum for $\alpha, \beta \in [0, \pi]$ for the orthogonal orientation with $\alpha = \beta = \pi/2$. Here, the time till the maximum entanglement is given by

$$t_{\max} = \frac{4\pi\hbar L^3}{GM_A M_B \Delta x_A \Delta x_B} \simeq 129\,\mathrm{mn} \tag{5.3}$$

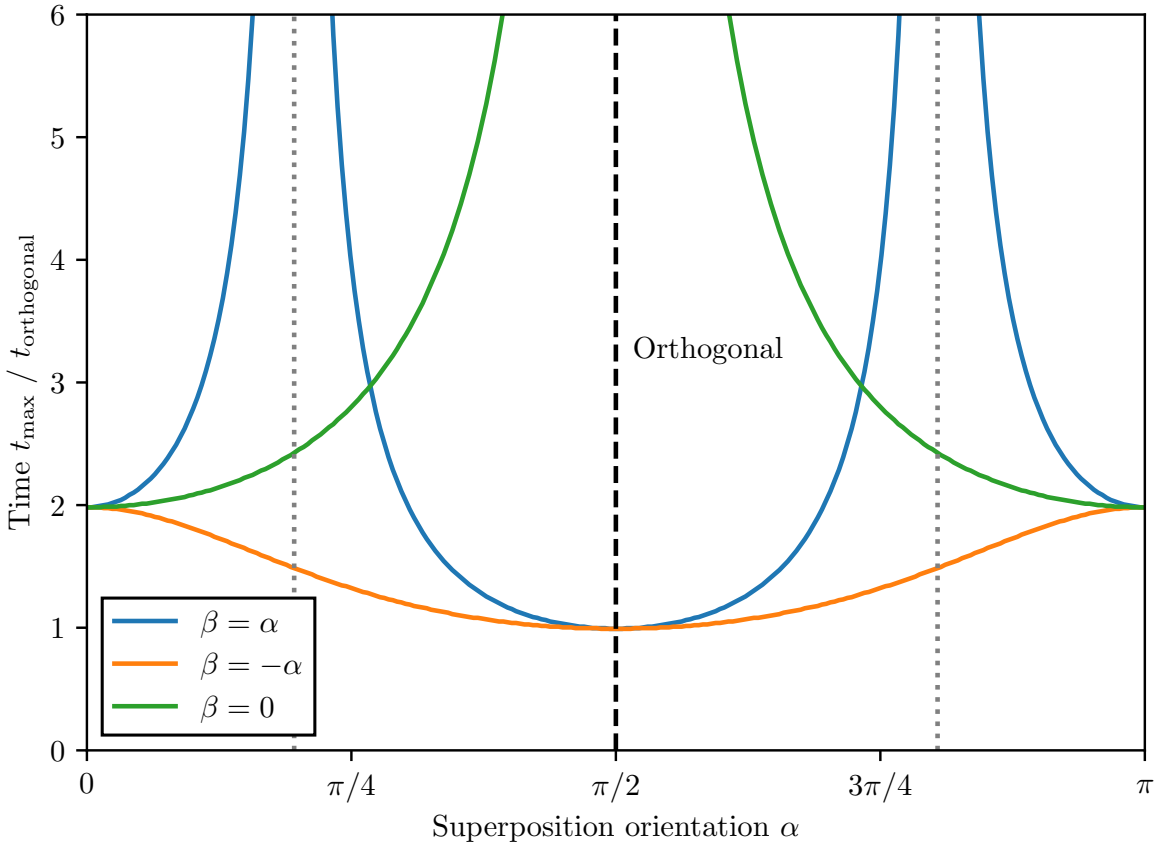

Figure 5.2: ...

Bibliography

[1] T. Krisnanda, G. Y. Tham, M. Paternostro, and T. Paterek, "Observable quantum entanglement due to gravity", npj Quantum Information **6**, 10.1038/s41534-020-0243-y (2019) 10.1038/s41534-020-0243-y, arXiv:1906.08808.

[2] H. Chevalier, A. J. Paige, and M. S. Kim, "Witnessing the nonclassical nature of gravity in the presence of unknown interactions", Physical Review A **102**, 022428 (2020) 10.1103/physreva.102.022428, arXiv:2005.13922.

[3] J. S. Pedernales, G. W. Morley, and M. B. Plenio, "Motional Dynamical Decoupling for Matter-Wave Interferometry", Phy. Rev. Lett. **125**, 023602 (2019) 10.1103/physrevlett.125.023602, arXiv:1906.00835.

[4] S. Bose, A. Mazumdar, G. W. Morley, H. Ulbricht, M. Toroš, M. Paternostro, A. Geraci, P. Barker, M. S. Kim, and G. Milburn, "A Spin Entanglement Witness for Quantum Gravity", Phys. Rev. Lett. **119**, 240401 (2017) 10.1103/physrevlett.119.240401, arXiv:1707.06050.

[5] L. Lami, J. S. Pedernales, and M. B. Plenio, "Testing the quantum nature of gravity without entanglement", Phys. Rev. X **14**, 021022 (2023) 10.1103/physrevx.14.021022, arXiv:2302.03075.

[6] R. Horodecki, P. Horodecki, M. Horodecki, and K. Horodecki, "Quantum entanglement", Rev. Mod. Phys. **81**, 865–942 (2007) 10.1103/revmodphys.81.865, arXiv:quant-ph/0702225.

[7] M. B. Plenio and S. Virmani, "An introduction to entanglement measures", Quantum Information & Computation **7**, 1–51 (2005), arXiv:quant-ph/0504163.

[8] J. S. Pedernales and M. B. Plenio, "On the origin of force sensitivity in tests of quantum gravity with delocalised mechanical systems", Contemporary Physics **64**, 147–163 (2023) 10.1080/00107514.2023.2286074, arXiv:2311.04745.

[9] D. Carney, P. C. E. Stamp, and J. M. Taylor, "Tabletop experiments for quantum gravity: a user's manual", Classical and Quantum Gravity **36**, 034001 (2018) 10.1088/1361-6382/aaf9ca, arXiv:1807.11494.

[10] M. Christodoulou, A. Di Biagio, M. Aspelmeyer, Č. Brukner, C. Rovelli, and R. Howl, "Locally mediated entanglement in linearised quantum gravity", Physical Review Letters **130**, 100202 (2022) 10.1103/physrevlett.130.100202, arXiv:2202.03368.

[11] T. Westphal, H. Hepach, J. Pfaff, and M. Aspelmeyer, "Measurement of Gravitational Coupling between Millimeter-Sized Masses", Nature **591**, 225–228 (2021) 10.1038/s41586-021-03250-7, arXiv:2009.09546.

[12] H. B. G. Casimir, "On the attraction between two perfectly conducting plates", Proc. Kon. Ned. Akad. Wet. **51**, 793 (1948).

[13] H. B. G. Casimir and D. Polder, "The Influence of Retardation on the London-van der Waals Forces", Physical Review **73**, 360–372 (1948) 10.1103/physrev.73.360.

[14] L. Gurvits, "Classical deterministic complexity of Edmonds' problem and Quantum Entanglement", in Proceedings of the thirty-fifth annual acm symposium on theory of computing, Vol. 4, STOC03 (June 2003), pages 10–19, 10.1145/780542.780545, arXiv:quant-ph/0303055.

[15] G. Vidal and R. F. Werner, "A computable measure of entanglement", Phys. Rev. A **65**, 032314 (2001) 10.1103/physreva.65.032314, arXiv:quant-ph/0102117.

[16] M. Plenio, "Logarithmic negativity: a full entanglement monotone that is not convex.", Physical Review Letters **95**, 090503 (2005) 10.1103/PhysRevLett.95.090503, arXiv:quant-ph/0505071.

[17] T. W. van de Kamp, R. J. Marshman, S. Bose, and A. Mazumdar, "Quantum Gravity Witness via Entanglement of Masses: Casimir Screening", Phys. Rev. A **102**, 062807 (2020) 10.1103/physreva.102.062807, arXiv:2006.06931.

[18] F. London, "Zur Theorie und Systematik der Molekularkräfte", Zeitschrift für Physik **63**, 245–279 (1930) 10.1007/bf01421741.

[19] M. Bordag, U. Mohideen, and V. M. Mostepanenko, "New developments in the Casimir effect", Physics Reports **353**, 1–205 (2001) 10.1016/s0370-1573(01)00015-1, arXiv:quant-ph/0106045 [quant-ph].

[20] G. L. Klimchitskaya, U. Mohideen, and V. M. Mostepanenko, "The Casimir force between real materials: Experiment and theory", Reviews of Modern Physics **81**, 1827–1885 (2009) 10.1103/revmodphys.81.1827, arXiv:0902.4022.

[21] S. K. Lamoreaux, "The Casimir force: background, experiments, and applications", Reports on Progress in Physics **68**, 201–236 (2004) 10.1088/0034-4885/68/1/r04.

[22] M. Bordag, "Proceedings of the Fourth Workshop on Quantum Field Theory under the Influence of External Conditions", in The Casimir Effect 50 Years Later (June 1999), pages 1–410, 10.1142/9789814527576.

[23] L. H. Ford, "Casimir Force between a Dielectric Sphere and a Wall: A Model for Amplification of Vacuum Fluctuations", Phys. Rev. A **58**, 4279–4286 (1998) 10.1103/physreva.58.4279, arXiv:quant-ph/9804055.

[24] E. M. Lifshitz, "The theory of molecular attractive forces between solids", Sov. Phys. JETP **2**, 73–83 (1956) 10.1016/b978-0-08-036364-6.50031-4.

[25] M. Hartmann, "Casimir effect in the plane-spheregeometry: Beyond the proximityforce approximation", PhD thesis (Universität Augsburg, July 2018).

[26] T. Emig, "Fluctuation induced quantum interactions between compact objects and a plane mirror", Journal of Statistical Mechanics: Theory and Experiment **2008**, P04007 (2007) 10.1088/1742-5468/2008/04/p04007, arXiv:0712.2199.

[27] A. Bulgac, P. Magierski, and A. Wirzba, "Scalar Casimir effect between Dirichlet spheres or a plate and a sphere", Physical Review D **73**, 025007 (2006) 10.1103/physrevd.73.025007.

[28] A. Canaguier-Durand, R. Guérout, P. A. M. Neto, A. Lambrecht, and S. Reynaud, "The Casimir effect in the sphere-plane geometry", International Journal of Modern Physics Conference Series **14**, 250–259 (2012) 10.1142/s2010194512007374, arXiv:1202.3272.

[29] M. A. Nielsen and I. L. Chuang, ***Quantum computation and quantum information***, 10th anniversary ed. (Cambridge University Press, Cambridge, 2010), 1676 pages.

[30] G. A. E. Vandenbosch, "The basic concepts determining electromagnetic shielding", American Journal of Physics **90**, 672–681 (2022) 10.1119/5.0087295.

[31] D. J. Griffiths, ***Elektrodynamik, Eine Einführung***, edited by U. Schollwöck, 4th edition (Pearson, Hallbergmoos, 2018), 1711 pages.

[32] I. G. Pirozhenko and M. Bordag, "On the Casimir repulsion in sphere-plate geometry", Physical Review D **87**, 085031 (2013) 10.1103/physrevd.87.085031, arXiv:1302.5290.

[33] T. Emig, N. Graham, R. L. Jaffe, and M. Kardar, "Casimir forces between arbitrary compact objects", Phys. Rev. Lett. **99**, 170403 (2007) 10.1103/physrevlett.99.170403, arXiv:0707.1862.

A TITLE TO BE DONE

A.1 Evolution under a gravitational Hamiltonian

In this section the time evolution of a system under Hamiltonian eq. (2.3) is calculated a) using the gravitational interaction $\hat{H}_G$ as a perturbation b) using an exact time evolution of coherent states.

A.1.1 Using time dependent perturbation theory

A general biparty Fock state $|\psi_0\rangle = |kl\rangle$ with $k, l \in \mathbb{N}_0$ can be evolved in time under a Hamiltonian eq. (2.3) treating the gravitational interaction $H_G = -\hbar g(\hat{a}_1\hat{a}_2^\dagger + \hat{a}_1^\dagger\hat{a}_2)$ as a perturbation. The resulting state $|\psi(t)\rangle$ after some time t is in the most general form given as

$$|\psi(t)\rangle = \sum_{i,j\geq 0} c_{i,j}(t)\,|i,j\rangle \tag{A.1}$$

where the coefficients $c_{i,j}(t)$ are given by first order perturbation theory as

$$c_{i,j}(t) = c_{i,j}(t=0) - \frac{i}{\hbar}\int_0^t \mathrm{d}t'\,\langle ij|\,\hat{H}_G\,|kl\rangle\,e^{-i(E_{kl}-E_{ij})t'/\hbar}. \tag{A.2}$$

The exponent is given by the energy of the appropriate Fock states $E_{kl} - E_{ij} = \hbar\omega(k + l - (i + j))$ and the matrix element in the integrand can be calculated to

$$\langle ij|\,\hat{H}_G\,|kl\rangle = \begin{cases} -\hbar g & \text{if } i = k \pm 1 \text{ and } j = l \mp 1 \\ 0 & \text{otherwise} \end{cases}. \tag{A.3}$$

The coefficients for $t = 0$ are trivially given from the initial state as

$$c_{i,j}(t=0) = \begin{cases} 1 & \text{for } i,j = k,l \\ 0 & \text{otherwise} \end{cases}. \tag{A.4}$$

For the non-zero states the energies in the exponent equate to zero and the evolved state is given by (up to a normalization)

$$|\psi(t)\rangle = |kl\rangle - igt\,|k-1, l+1\rangle - igt\,|k+1, l-1\rangle + \mathcal{O}(g^2). \tag{A.5}$$

The result eq. (2.5) is represented by eq. (A.5) for the case of $k = 1$ and $l = 0$.

A.1.2 Using an exact time evolution

The Hamiltonian eq. (2.3) can be rewritten using symmetric and antisymmetric normal modes

$$\hat{a}_\pm = \frac{1}{\sqrt{2}}\left(\hat{a}_1 \pm \hat{a}_2\right) \tag{A.6}$$

in the form of

$$\hat{H} = \hbar\omega_+ \hat{a}_+^\dagger \hat{a}_+ + \hbar\omega_- \hat{a}_-^\dagger \hat{a}_-, \quad \omega_\pm = \omega \pm (-g) \tag{A.7}$$

The initial state consisting of two coherent oscillator states is in the new modes given by

$$|\psi(t)\rangle = |\alpha\rangle_1 |\beta\rangle_2 = \left|\frac{1}{\sqrt{2}}(\alpha+\beta)\right\rangle_+ \left|\frac{1}{\sqrt{2}}(\alpha-\beta)\right\rangle_- \tag{A.8}$$

A general coherent state $|\gamma\rangle$ evolves in time under an Hamiltonian $\hat{H} = \hbar\omega\hat{a}^\dagger\hat{a}$ like $|\gamma(t)\rangle = |e^{-i\omega t}\gamma\rangle$ which can be used to evolve the state in eq. (A.8):

$$|\psi(t)\rangle = \left|\frac{1}{\sqrt{2}} e^{-i\omega_+ t}(\alpha+\beta)\right\rangle_+ \left|\frac{1}{\sqrt{2}} e^{-i\omega_- t}(\alpha-\beta)\right\rangle_- \tag{A.9}$$

$$= \left|e^{-i\omega t}\left(\alpha\cos gt - \beta\sin gt\right)\right\rangle_1 \left|e^{-i\omega t}\left(-\alpha\sin gt + \beta\cos gt\right)\right\rangle_2, \tag{A.10}$$

where in the last line the back-transformation from the $\pm$-modes (A.8) was used.

A.2 Exemplary calculation of E_N

In this section, the logarithmic negativity E_N eq. (2.21) is exemplary calculated for the state eq. (2.13). The density matrix of this system is given by

$$\rho(t) = |\psi(t)\rangle\langle\psi(t)| = \frac{1}{4}\begin{pmatrix} 1 & e^{i\Delta\phi} & e^{i\Delta\phi} & 1 \\ e^{-i\Delta\phi} & 1 & 1 & e^{-i\Delta\phi} \\ e^{-i\Delta\phi} & 1 & 1 & e^{-i\Delta\phi} \\ 1 & e^{i\Delta\phi} & e^{i\Delta\phi} & 1 \end{pmatrix}. \tag{A.11}$$

Consequently, the partially transposed density ρ^{Γ_B} is given by

$$\rho^{\Gamma_B}(t) = \frac{1}{4}\begin{pmatrix} 1 & e^{-i\Delta\phi} & e^{i\Delta\phi} & 1 \\ e^{i\Delta\phi} & 1 & 1 & e^{-i\Delta\phi} \\ e^{-i\Delta\phi} & 1 & 1 & e^{i\Delta\phi} \\ 1 & e^{i\Delta\phi} & e^{-i\Delta\phi} & 1 \end{pmatrix}. \tag{A.12}$$

The eigenvalues where calculated using `Mathematica` and equate to

$$\left\{\sin^2\left(\frac{\Delta\phi}{2}\right), \cos^2\left(\frac{\Delta\phi}{2}\right), \frac{\sin\Delta\phi}{2}, -\frac{\sin\Delta\phi}{2}\right\}$$

According to lemma 2.1, $\left\|\rho^{\Gamma_B}\right\|_1$ is given by the sum of the absolute eigenvalues, which is equal to $1 + |\sin \Delta\phi|$. The negativity as the absolute sum of all negative eigenvalues (demonstrated in proposition 2.3) equates to $\mathcal{N} = |\sin \Delta\phi| /2$. Both methods result in a logarithmic negativity of $E_N = \log_2(1 + |\sin \Delta\phi|)$.

B Casimir interactions

B.1 Polarizability of a dielectric sphere

The polarizability α is defined via

$$\mathbf{E}_\infty \alpha = \mathbf{p}, \tag{B.1}$$

where $\mathbf{p}$ is the induced dipole moment and $\mathbf{E}_\infty$ is the external electric field that induces the dipole moment. For a linear and uniform dielectric, it is given as $\mathbf{p} = \mathcal{V}\varepsilon_0(\varepsilon_r - 1)\mathbf{E}_{\text{in}}$ [31, p. 220-226]. Here, $\mathcal{V}$ is the volume of the object and $\mathbf{E}_{\text{in}}$ is the electric field inside the dielectric. The electrostatic boundary conditions for the problem are given by

$$V_{\text{in}}\Big|_{r=R} = V_{\text{out}}\Big|_{r=R} \quad \text{and} \quad \varepsilon_r\varepsilon_0 \frac{\partial V_{\text{in}}}{\partial r}\bigg|_{r=R} = \varepsilon_0 \frac{\partial V_{\text{out}}}{\partial r}\bigg|_{r=R} \tag{B.2}$$

and the electric potential outside of the sphere at $r \to \infty$ should be equal to the external dipole-inducing field $V_{\text{out}}|_{r\to\infty} = -\mathbf{E}_\infty \cdot \mathbf{r} = -E_\infty r\cos\theta$. The electric potential inside and outside the sphere can be calculated using the spherical decomposition of the general electric potential $V \propto 1/|\mathbf{r} - \mathbf{r}'|$ into Legendre Polynomials P_l [31, p. 188-190]:

$$V_{\text{in}}(r,\theta) = -E_\infty r\cos\theta + \sum_{l=0}^{\infty} A_l r^l P_l(\cos\theta), \tag{B.3}$$

$$V_{\text{out}}(r,\theta) = -E_\infty r\cos\theta + \sum_{l=0}^{\infty} \frac{B_l}{r^{l+1}} P_l(\cos\theta). \tag{B.4}$$

Applying both boundary conditions, it follows that [31, p. 249-251]

$$\begin{cases} A_l = B_l = 0 & \text{for } l \neq 1, \\ A_1 = -\frac{3}{\varepsilon_r+2}E_\infty, \quad B_1 = \frac{\varepsilon_r-1}{\varepsilon_r+2}R^3 E_\infty \end{cases} \tag{B.5}$$

and the resulting homogenous electric field $\mathbf{E}_{\text{in}} = -\nabla V_{\text{in}}$ inside the sphere is given as

$$\mathbf{E}_{\text{in}} = \frac{3}{\varepsilon_r + 2}\mathbf{E}_\infty. \tag{B.6}$$

The field is shown on the right in fig. B.1.The polarizability α of the sphere can be now be determined to

$$\alpha_{\text{sphere}} = 4\pi\varepsilon_0 R^3 \left(\frac{\varepsilon_r - 1}{\varepsilon_r + 2}\right). \tag{B.7}$$

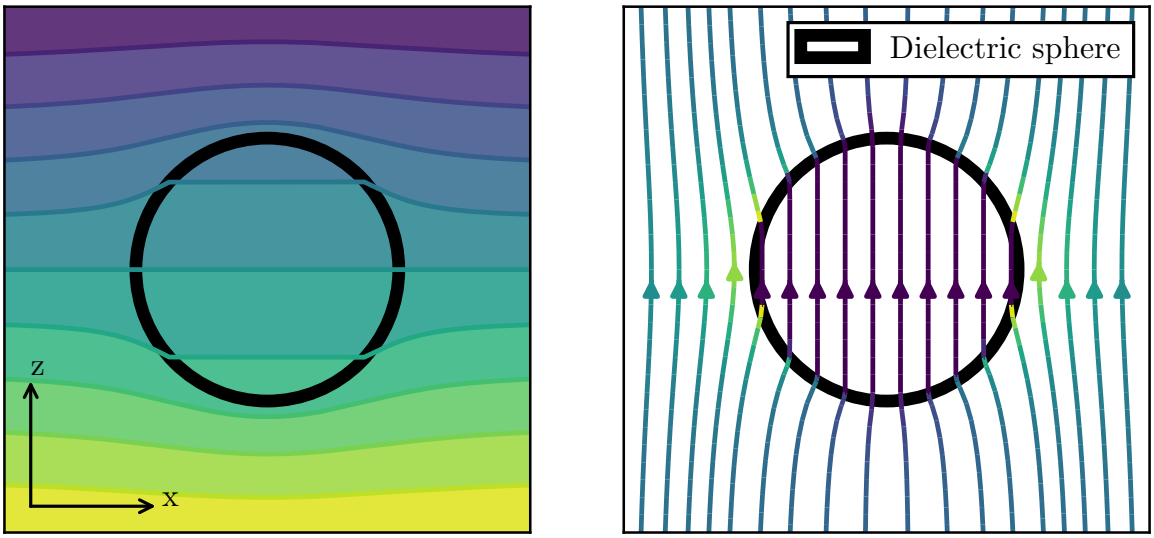

Figure B.1: left: Electric potential V of a dielectric sphere in a external electric field $\mathbf{E}_\infty \parallel \mathbf{e_z}$. **right:** The corresponding electric field lines inside and outside the dielectric sphere.

C The shield and its consequences

C.1 Thermal harmonic oscillator

TO BE MADE